AIAA JOURNAL
Vol. 31, No. 1, January 1993

Eduction of Swirling Structure Using the Velocity Gradient Tensor

C. H. Berdahl* and D. S. Thompson†
University of Texas at Arlington, Arlington, Texas 76019

In this paper we propose a technique for locating swirling regions of a flowfield. The technique is based on the eigenvalues of the velocity gradient tensor. We show that regions of swirling flow are characterized by complex eigenvalues for a constant velocity gradient tensor. Using results obtained in this analysis, we define an approximate parameter to indicate the tendency for the fluid to swirl about the point in question. The technique is illustrated by application to several two- and three-dimensional flowfields. In addition, the basic ideas contained here suggest the existence of a fluid property that we have termed intrinsic swirl. This new property may also be useful for control of fluid motion in many practical problems.

Introduction

MANY flows have a rich variety of structure. Vortices and shock waves provide the basic building blocks for much of this structure. Fluid dynamicists frequently attempt to characterize these structures to understand the behavior of a given flowfield. In experimental fluid dynamics, where sophisticated measurement techniques can produce a large amount of extremely detailed flowfield information, this characterization can present quite a problem. Computational fluid dynamics (CFD) flow solutions present essentially the same problem for two reasons. The first is increased computational power that enables better resolution of significant flow features with finer grids. A second reason is that CFD modeling techniques now include more of the physics of the flow. Flow fields such as turbulent shear layers or delta wings at angle of attack contain complex vortical structure and are typically computed on grids containing hundreds of thousands if not millions of points. Computation of such flows has given new urgency to the need for flow visualization algorithms. In fact, an entire session was devoted to this topic at the AIAA 8th CFD Conference in 1987.[1-4]

Of particular interest is the difficulty of locating a vortex—a simple form of swirling motion. A vortex is sometimes identified by the existence of a local extremum in the vorticity.[5] However, this is not a necessary condition for the existence of a vortex. Conventional thought would maintain that the vorticity describes "rotation" of a fluid in a differential or point sense. However, according to Truesdell,[6] the notion of vorticity came into mainstream fluid dynamics thought after a great deal of controversy. The bulk swirling motion we are referring to is obviously quite different from the type of rotation described by the concept of vorticity.

In this paper we propose a new method for determining the location of swirling regions of flow. We define swirling flow to be any fluid motion that suggests rotation of fluid particles about a common center, either fixed or moving. This definition is constructed so as to include vortices and eddies. The method, motivated by Berdahl and Strang,[7] is based on properties of the velocity gradient tensor. In regions of swirling flow, the eigenvalues of the velocity gradient tensor are complex. Thus, regions of swirling flow can be discerned by locating regions of complex eigenvalues.

It should be noted that previous workers have attempted to classify swirling motion using critical point concepts and autonomous ordinary differential equations. Perry and Chong[8] show that the fluid exhibits swirling motion near critical points when the velocity gradient tensor has complex eigenvalues. Their analysis relies on finding critical points in a flow to sketch the basic structure of the flow. The reader is referred to this paper for a review of current ideas on this topic.

Background

The velocity gradient tensor fully describes the spatial variation of the velocity vector to first order. Following Thompson,[9] the velocity of a particle at $\boldsymbol{x}+\mathrm{d}\boldsymbol{x}$ relative to that at $\boldsymbol{x}$ is given by

$$\mathrm{d}u_i = \frac{\partial u_i}{\partial x_k}\,\mathrm{d}x_k \tag{1}$$

where $\partial u_i/\partial x_k$ is the velocity gradient tensor ($i=1,2,3$ and $k=1,2,3$). Equation (1) can be written in vector/tensor form as

$$\mathrm{d}\boldsymbol{u} = \boldsymbol{L}\,\mathrm{d}\boldsymbol{x} \tag{2}$$

where $\boldsymbol{L}$ is the matrix representation of the velocity gradient tensor. Providing $\boldsymbol{L}$ has a complete set of linearly independent eigenvectors, a similarity transformation exists[10] such that

$$\boldsymbol{L} = \boldsymbol{T}\boldsymbol{\Lambda}\boldsymbol{T}^{-1} \tag{3}$$

where $\boldsymbol{\Lambda}$ is a diagonal matrix of the eigenvalues of $\boldsymbol{L}$, as in $\boldsymbol{\Lambda} = \mathrm{diag}(\lambda_1, \lambda_2, \lambda_3)$, and $\boldsymbol{T}$ is a matrix with columns that are the right, or column, eigenvectors of $\boldsymbol{L}$ taken in the same order as the eigenvalues in $\boldsymbol{\Lambda}$

$$\boldsymbol{T} = [\boldsymbol{r}_1\boldsymbol{r}_2\boldsymbol{r}_3] \tag{4}$$

with $\boldsymbol{r}_i$ ($i=1,2,3$) being the column eigenvectors of $\boldsymbol{L}$, and $\boldsymbol{T}^{-1}$ is a matrix with rows that are the left, or row, eigenvectors of $\boldsymbol{L}$ taken in the same order as the eigenvalues in $\boldsymbol{\Lambda}$

$$\boldsymbol{T}^{-1} = \begin{bmatrix} \boldsymbol{l}_1 \\ \boldsymbol{l}_2 \\ \boldsymbol{l}_3 \end{bmatrix} \tag{5}$$

*Presented as Paper 91-1823 at the AIAA 22nd Fluid Dynamics, Plasma Dynamics, and Lasers Conference, Honolulu, HI, June 24-26, 1991; received July 19, 1991; revision received June 20, 1992; accepted for publication June 24, 1992.

*Graduate Student, Department of Aerospace Engineering; currently First Officer, American Airline Flight Operations, American Airlines, Boston, MA. Member AIAA.

†Assistant Professor, Department of Aerospace Engineering. Member AIAA.

with l_i ($i = 1,2,3$) being the row eigenvectors of $\boldsymbol{L}$. Premultiplying Eq. (2) by $\boldsymbol{T}^{-1}$ yields

$$\boldsymbol{T}^{-1}\,\mathrm{d}\boldsymbol{u} = \boldsymbol{\Lambda}\boldsymbol{T}^{-1}\,\mathrm{d}\boldsymbol{x} \tag{6}$$

or

$$\mathrm{d}\boldsymbol{w} = \boldsymbol{\Lambda}\,\mathrm{d}\boldsymbol{X} \tag{7}$$

where $\mathrm{d}\boldsymbol{w} = \boldsymbol{T}^{-1}\,\mathrm{d}\boldsymbol{u}$ and $\mathrm{d}\boldsymbol{X} = \boldsymbol{T}^{-1}\,\mathrm{d}\boldsymbol{x}$. Equation (7) shows that $\mathrm{d}\boldsymbol{w}$ is parallel to $\mathrm{d}\boldsymbol{X}$. These "characteristic" directions are defined by the "transformation matrix" $\boldsymbol{T}^{-1}$. The behavior of this transformation is clear when the eigenvalues of $\boldsymbol{L}$ are real. Of interest here is the interpretation when the eigenvalues are complex.

At this point, a digression to the literature is appropriate. For convenience, the velocity gradient tensor can be split into symmetric and antisymmetric parts[9,11] as

$$\frac{\partial u_i}{\partial x_k} = \frac{1}{2}\left(\frac{\partial u_i}{\partial x_k} + \frac{\partial u_k}{\partial x_i}\right) + \frac{1}{2}\left(\frac{\partial u_i}{\partial x_k} - \frac{\partial u_k}{\partial x_i}\right) \tag{8}$$

The first tensor on the right side of Eq. (8) is the deformation tensor and the second is the spin tensor. Because of the antisymmetry of the spin tensor, only three independent components are required to fully define it. The three components of the spin tensor are the components of the vorticity vector. Since the deformation tensor is real and symmetric, the associated eigenvalues and eigenvectors are real. The fluid motion can be thought of as being extensive in the directions implied by the eigenvectors with an added rotation that is the vorticity.

The more general case concerns the behavior of the intact velocity gradient tensor $\boldsymbol{L}$. When the eigenvalues of $\boldsymbol{L}$ are real, the diagonalization of Eq. (6) exists with the directions given by the rows of the "transformation matrix" $\boldsymbol{T}^{-1}$. The off-diagonal terms of the velocity gradient tensor are zero in this coordinate system. When the eigenvalues are complex, no physical transformation of the coordinate system diagonalizes the velocity gradient tensor. When the off-diagonal components of the velocity gradient tensor cannot be made zero by a fortuitous selection of coordinate system, the flowfield at the point in question exhibits a behavior that we have termed intrinsic swirl.

Complex Eigenvalues

It is now appropriate to present some preliminary ideas concerning the conditions under which the eigenvalues of the velocity gradient tensor are complex.

Irrotational Flows

In an irrotational flow, the spin tensor in Eq. (8) is identically zero. The velocity gradient tensor is therefore real and symmetric and has real eigenvalues. Therefore, a necessary condition for the existence of complex eigenvalues is that the velocity field must have nonzero vorticity.

Rotational Flows

For the case of two-dimensional flow, the characteristic equation of the velocity gradient tensor can be written as

$$\lambda^2 - \mathrm{tr}\boldsymbol{L}\,\lambda + \det\boldsymbol{L} = 0 \tag{9}$$

where $\mathrm{tr}\boldsymbol{L}$ is the trace of the velocity gradient tensor and $\det\boldsymbol{L}$ is the determinant. It should be noted that $\mathrm{tr}\boldsymbol{L} = \mathrm{div}\boldsymbol{V}$. Equation (9) is a quadratic equation for λ. Thus, the eigenvalues of $\boldsymbol{L}$ are complex if

$$(\tfrac{1}{2}\mathrm{div}\boldsymbol{V})^2 - \det\boldsymbol{L} < 0 \tag{10}$$

For the special case of two-dimensional Cartesians, Eq. (10) reduces to

$$\tfrac{1}{4}(u_x + v_y)^2 - (u_x v_y - u_y v_x) < 0 \tag{11}$$

or

$$u_y v_x < -\tfrac{1}{4}(u_x - v_y)^2 \tag{12}$$

Equation (12) is satisfied only when the shearing strain rates u_y and v_x are of opposite signs and their product larger in magnitude than the right side of the equation. In incompressible flow, $\mathrm{div}\boldsymbol{V} = 0$ so that the preceding condition reduces to

$$\det\boldsymbol{L} > 0 \tag{13}$$

or, for two-dimensional Cartesians,

$$u_y v_x < u_x v_y \tag{14}$$

Since we are dealing with incompressible motion, the normal strain rates u_x and v_y are of equal magnitude and opposite sign so that the shearing strain rates again must be of opposite signs and their product must be larger in magnitude than the product of the normal strain rates.

If the fluid motion is three dimensional, the characteristic equation can be written as

$$-\lambda^3 + \mathrm{tr}\boldsymbol{L}\,\lambda^2 - \tfrac{1}{2}[(\mathrm{tr}\boldsymbol{L})^2 - \mathrm{tr}\boldsymbol{L}^2]\lambda + \det\boldsymbol{L} = 0 \tag{15}$$

Two of the roots of this cubic equation are complex conjugates provided the coefficients of the equation satisfy certain conditions. The resulting inequality is relatively complex and is not included since no additional insights have been gleaned from it to date. If the flowfield is incompressible, the condition under which two of the roots are complex conjugates is simplified somewhat and is given by

$$(\det\boldsymbol{L})^2 - \frac{1}{54}(\mathrm{tr}\boldsymbol{L}^2)^3 > 0 \tag{16}$$

This result is included primarily for completeness since this relationship has, as yet, not provided any useful information.

Motion with Constant Velocity Gradient Tensor

We now present an example that illustrates the connection between "swirling" motion and complex eigenvalues. In addition, the role played by the eigenvectors is clarified. Assume that the components of the velocity gradient tensor are temporally and spatially constant. Movement of a particle around the origin then reduces to the system of first-order, linear differential equations with constant coefficients given by

$$\frac{\mathrm{d}\boldsymbol{x}}{\mathrm{d}t} = \boldsymbol{L}\boldsymbol{x} \tag{17}$$

where $\boldsymbol{L}$ is the velocity gradient tensor and $\boldsymbol{x}$ the position vector from the origin. The initial condition is given by $\boldsymbol{x}(0) = \boldsymbol{x}_0$ where $\boldsymbol{x}_0$ is the initial position of the particle with respect to the origin. If complex eigenvalues do occur, all three of the eigenvalues are unique. Therefore, it is possible to use Eq. (3) to decompose $\boldsymbol{L}$ since eigenvectors corresponding to unique eigenvalues are linearly independent.[10] Equation (17) can then be written as

$$\frac{\mathrm{d}\boldsymbol{x}}{\mathrm{d}t} = \boldsymbol{T}\boldsymbol{\Lambda}\boldsymbol{T}^{-1}\boldsymbol{x} \tag{18}$$

By defining $\boldsymbol{X} = \boldsymbol{T}^{-1}\boldsymbol{x}$ and recalling that the elements of $\boldsymbol{L}$ are assumed spatially and temporally constant, we obtain

$$\frac{\mathrm{d}\boldsymbol{X}}{\mathrm{d}t} = \boldsymbol{\Lambda}\boldsymbol{X} \tag{19}$$

The important point to be made here is that the system is now decoupled since $\boldsymbol{\Lambda}$ is a diagonal matrix. The solution is easily obtained to be[10]

$$\boldsymbol{X}(t) = e^{\boldsymbol{\Lambda}t}\boldsymbol{X}_0 \tag{20}$$

where $e^{\Lambda t} = \text{diag}(e^{\lambda_1 t}, e^{\lambda_2 t}, e^{\lambda_3 t})$ and $X_0 = T^{-1}x_0$. Performing the indicated multiplication yields

$$X(t) = \begin{Bmatrix} X_1(t) \\ X_2(t) \\ X_3(t) \end{Bmatrix} = \begin{Bmatrix} e^{\lambda_1 t} X_{0_1} \\ e^{\lambda_2 t} X_{0_2} \\ e^{\lambda_3 t} X_{0_3} \end{Bmatrix} \tag{21}$$

The solution given in Eq. (21) consists of three decoupled motions in the complex plane. The elements of the vector X_0, X_{0_1}, X_{0_2}, and X_{0_3} represent the initial points of the three trajectories. For convenience, we will assume that λ_1 and λ_2 are the complex conjugate pair. This assumption implies that λ_3 is purely real. $X_1(t)$ and $X_2(t)$ are spiraling motions in the complex plane with amplitudes that decay or grow depending on the sign of the real part of the complex conjugate eigenvalues. If the real part is identically zero, circular paths are obtained in the complex plane. A period for this motion, i.e., the time for return to the same angular position, can be computed using

$$t_{\text{orbit}} = \frac{2\pi}{|\text{Im}(\lambda_{1,2})|} \tag{22}$$

The remaining eigenvalue λ_3 yields an exponentially decaying or growing solution $X_3(t)$ along the real axis.

The solution in physical space is obtained using the inverse mapping

$$x(t) = TX(t) \tag{23}$$

After performing the indicated multiplications, the solution can be written as

$$x(t) = r_1 e^{\lambda_1 t} X_{0_1} + r_2 e^{\lambda_2 t} X_{0_2} + r_3 e^{\lambda_3 t} X_{0_3} \tag{24}$$

The right eigenvectors "map" the three motions in the complex plane to the motion in the physical plane. r_1 and r_2 are a conjugate pair, as are l_1 and l_2, so that the result of Eq. (24) is real. For two-dimensional motion, the real eigenvalue is zero and the third dimension decouples because of the form of the left and right eigenvectors.

We have established the connection between swirling motion and complex eigenvalues for a very special case—a velocity field with a constant velocity gradient tensor. In the next section we outline a technique based on the preceding development that we have found useful for locating regions of swirling motion for realistic flowfields.

Intrinsic Swirl Parameter

The major caveat associated with identifying swirling regions of the flowfield as regions where the eigenvalues of the velocity gradient tensor are complex is that it is possible for a fluid particle to convect out of a region of complex eigenvalues before swirling motion is apparent. However, if the fluid particle is moving "slowly," relatively speaking, the particle may be "captured" by the vortex. Thus, the convection velocity plays an important role in determining which regions of the fluid having complex eigenvalues exhibit swirling motion.

Using the results of Eq. (22), we can define a nondimensional "intrinsic swirl" parameter τ that is the ratio of the time for a fluid particle to convect through the region of complex eigenvalues to the orbit time

$$\tau = \frac{t_{\text{conv}}}{t_{\text{orbit}}} \tag{25}$$

By defining $t_{\text{conv}} = L/V_{\text{conv}}$, where L is a characteristic length associated with the size of the region of complex eigenvalues, V_{conv} is the magnitude of the velocity aligned along L, and using Eq. (22), we obtain

$$\tau = \frac{|\text{Im}(\lambda_{1,2})|L}{2\pi V_{\text{conv}}} \tag{26}$$

In regions where $\tau \to 0$, the fluid convects too rapidly through the region of complex eigenvalues to be "captured" in swirling motion. In regions where $\tau \gg 0$, the fluid does not move quickly enough and is trapped in a swirling motion.

An additional point to consider is that, in general, the length and orientation of L are unknown. In two dimensions, it is clear that the relevant velocity is contained in the plane of motion. In addition, it would seem that using the magnitude of the velocity would provide the most conservative estimate. In three dimensions, the problem is much more complex since, in general, there is no "plane of swirling motion" except for simple flowfields. In two dimensions, the vorticity vector and the real eigenvector r_3 are parallel to the normal to the plane containing the motion. The three-dimensional analogy would be the velocity in the plane whose normal is parallel to the vorticity vector or, possibly the real eigenvector as in

$$V_{\text{conv}}^2 = V^2 - (\hat{n} \cdot V)^2 \tag{27}$$

where $\hat{n}$ is the vector corresponding to either the normalized vorticity vector $\omega/|\omega|$ or the normalized real eigenvector $r_3/|r_3|$. Of course, the orientation of this plane varies from point to point in the flowfield based on the local velocity gradient tensor. A third possibility is to map the physical velocity to the complex plane using either of the normalized conjugate left eigenvectors and to use the magnitude of the complex velocity

$$V_{\text{conv}}^2 = |\bar{l}_{1,2}^T \cdot V| \tag{28}$$

The advantage in using this approach is that very intricate three-dimensional motions are reduced to planar trajectories as suggested by Eq. (24). Therefore, a "plane of swirling motion" is defined—albeit the complex plane. It is not known a priori which of these methods will work best and results using all three will be presented. None of these approaches address the selection of L. To date, we have taken L to be unity.

It should be realized that this parameter is approximate in the sense that the expression for the orbit time is based on a constant velocity gradient tensor. In other words, we are attempting to use a local quantity to describe a global motion. We interpret τ on a point-to-point basis as the tendency for the fluid to swirl about the point in question. The parameter is effective for locating the "most active" swirling structures. A second point is that the intrinsic swirl parameter τ is reference-frame dependent through the convection velocity V_{conv} whereas the velocity gradient tensor is independent of the reference frame, providing the reference frame is not accelerating. Therefore, for some types of problems, i.e., mixing flows, etc., it may be advantageous to define the convection velocity relative to a moving structure such as an eddy.

Implementation

Before presenting actual results, we would like to comment on several aspects of our implementation of the swirling flow eduction technique. The velocity gradients are computed in computational space using second-order central differences at field points and first-order, one-sided differences at boundary points. The derivatives are transformed to physical space using metrics computed in the same fashion as the velocity gradients. This brings up the second major caveat for using this method—the computed flowfield should be reasonably oscillation free. Since a nonphysical oscillation can cause a change in sign in the velocity gradients, the net result could be a region of spurious complex eigenvalues. The eigenvalues and right eigenvectors were computed numerically using the EISPACK library.[12] The inversion required to compute the matrix of left eigenvectors from the right eigenvector matrix was performed using the LINPACK library.[13]

Application of Method

The swirling flow eduction technique is now applied to several different flowfields to illustrate the major points discussed earlier.

Examples 1 and 2—Driven Cavity

The flow in a driven cavity of aspect ratio two was computed using the vorticity-stream function version of the incompressible Navier-Stokes equations for two different Reynolds numbers, $Re = 1 \times 10$ and 2×10^2. An explicit, second-order central-difference[14] scheme was used to compute both solutions on the same 101×201 grid with $\Delta x = \Delta y = \text{const}$.

Figure 1 shows a plot of the lines of equal vorticity superimposed over a shaded contour plot of the magnitude of the complex eigenvalue field. As expected, the low Reynolds number results in a nearly symmetric flowfield. It is clear from this figure that the property we have denoted as intrinsic swirl is different from the vorticity. There are regions of nonzero vorticity that have real eigenvalues. This vorticity can be "removed" by transformation to the system of characteristic directions implied by the real eigenvectors since the velocity gradient tensor in the new basis system has zero off-diagonal components.

Figure 2 shows a plot of the streamlines superimposed over a shaded contour plot of the intrinsic swirl parameter τ for $Re = 1 \times 10$. The complex eigenvalues appear in the core region of the primary vortex as well as the core region of the secondary vortex. The streamline plot does not show the secondary vortex because of the small magnitude of the stream function in the region of secondary flow. In addition, the intrinsic swirl parameter and streamline plots indicate the presence of vortices in the lower left and right corners of the cavity. The utility of the intrinsic swirl parameter is evident from the fact that the magnitude of τ is largest in the core regions of the vortices.

Figure 3 shows a plot of the lines of equal vorticity superimposed over a shaded contour plot of the complex eigenvalue field for $Re = 2 \times 10^2$. At the higher Reynolds number the flowfield exhibits the expected asymmetry. Of interest is the region of real eigenvalues protruding into the imaginary region near $x = 0.3$ and $y = 1.9$. The existence of this region is due to the shifting of the vortex core to the right at the higher Reynolds number. Examination of the strain rates in this region showed that, generally, the magnitude of one of the shearing strain rates was very small in comparison with the other shearing rate and the normal strain rates so that Eq. (14) was not satisfied and the eigenvalues were real.

Figure 4 shows a plot of the streamlines superimposed over a shaded contour plot of the intrinsic swirl parameter. At the higher Reynolds number, the asymmetry of the flowfield is evident. Again the intrinsic swirl parameter locates the primary and secondary vortices as well as the vortices in the lower corners. As before, the cores of the vortices are clearly indicated. The utility of the intrinsic swirl parameter is again illustrated by the fact that the region of complex eigenvalues near the left wall at $y = 1.8$ is not highlighted in Fig. 4,

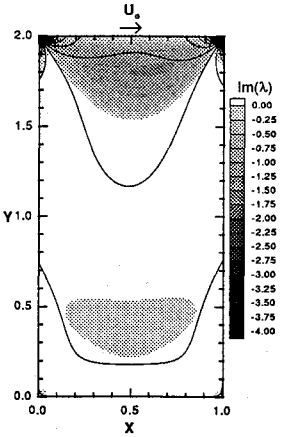

Fig. 1 Complex eigenvalue field and vorticity contours for driven cavity flow, $Re = 1 \times 10$.

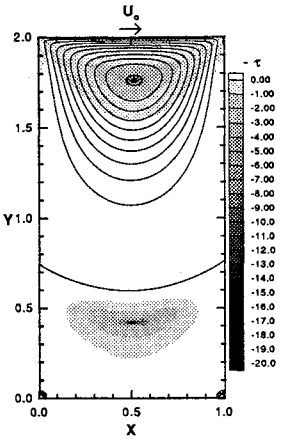

Fig. 2 Intrinsic swirl parameter and streamlines for driven cavity flowfield, $Re = 1 \times 10$.

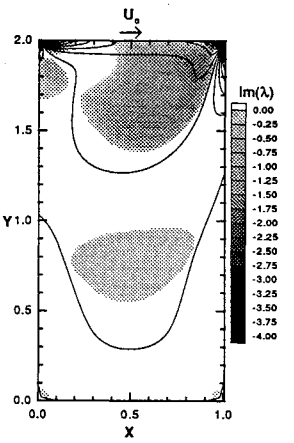

Fig. 3 Complex eigenvalue field and vorticity contours for driven cavity flow, $Re = 2 \times 10^2$.

whereas it appears as a darker region in Fig. 3, which does not take into account the convection velocity.

Example 3—Sonic Jet in Supersonic Crossflow

The technique is now applied to the two-dimensional flowfield due to a sonic jet in a supersonic crossflow ($M_\infty = 2.61$) reported in Ref. 15. The laminar solution was computed using an upwind-relaxation scheme on a 101×61 adaptive grid. Since this flowfield is compressible, the value of $\text{div}\boldsymbol{V}$ may be significantly different from zero. A plot of the pressure field and selected particle trajectories for the flowfield is shown in Fig. 5. The jet is located from $0.275 \leq x \leq 0.325$. Of particular interest here are the recirculating regions just upstream and downstream of the jet.

Figure 6 shows a plot of the velocity vectors and a shaded contour plot of the imaginary part of the conjugate eigenvalues for the region near the jet. The regions near A and B in the figure correspond to portions of the recirculating regions shown in Fig. 5. Examination of the particle paths near C and D shows that these regions do exhibit recirculating motion. These vortices are not apparent from a cursory examination of the velocity vectors. The region near E is located in the general recirculating region to the left of the jet. At a point just to the left of region E, $u < 0$ and $v < 0$, whereas just to the right, $u < 0$ and $v > 0$. Particles moving through this region from right to left experience an upward deflection and then a downward deflection just as particles in swirling motion would. However, the wall precludes a closed path from existing. A similar argument can be developed for region F. In the region labeled G, the magnitude of the complex eigenvalue is very small because of small velocity gradients existing in the area

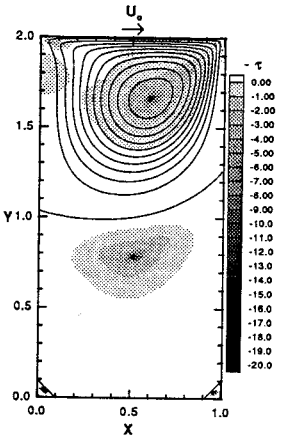

Fig. 4 Intrinsic swirl parameter and streamlines for driven cavity flowfield, $Re = 2 \times 10^2$.

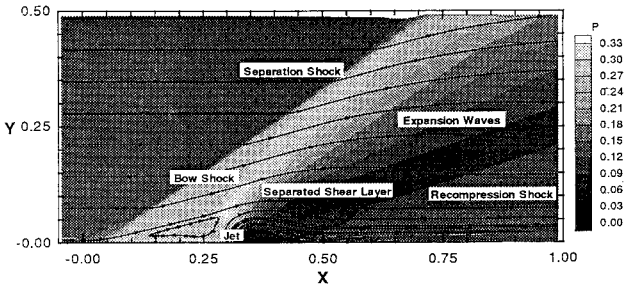

Fig. 5 Major features of sonic jet in supersonic crossflow.

between the shock and the shear layer. In addition, there are regions of complex eigenvalues that exist upstream of the shock because of spurious oscillations of very small magnitude that exist in the solution.

The region labeled H is best explained with reference to Fig. 7, which shows a contour plot of the intrinsic swirl parameter (shaded regions). In this figure, we see that the magnitude of τ is small in the separated shear layer in comparison with the magnitude of τ in the recirculating regions. In our interpretation, the region in the shear layer shows far less tendency to exhibit swirling motion than in the recirculating regions. Particle paths in the shear layer do not complete orbits since the orbital period is significantly larger than the convection time for fluid particles through the region. The intrinsic swirl parameter clearly locates the core regions of the swirling flows at A and B as well as the small recirculating regions at C and D.

Example 4—Delta Wing at Angle of Attack

The swirling flow eduction technique is now applied to the thin-layer Navier-Stokes calculation of flow over a delta wing with a leading edge sweep angle Γ of 75 deg and a leading edge vertex angle β of 35 deg performed by Webster and Shang.[16] The conditions for the particular case we chose were $M_\infty = 1.95$, $Re = 4.48 \times 10^6$, and $\alpha = 30$ deg. The laminar solution was computed on a $110 \times 80 \times 80$ grid using the ARC3D code,[17] a central-difference, approximate factorization code using user-specified artificial dissipation. The reader is referred to Ref. 16 for additional details concerning the delta wing geometry, the grid, and the flowfield calculations.

A simulated surface oil flow pattern for the delta wing is shown in Fig. 8. The simulated oil flow pattern shows a complex flowfield with significant chordwise flow reversal extending from the trailing edge forward to approximately 67% of the root chord.[16] In addition, two vortical structures are visible on each half of the wing. The streamwise station (station 30 or $X/L = 0.825$ with L being the centerline chord length) where the method is applied is also indicated. It should be noted that the "trailing edge" of the delta wing shown in Fig. 8 is actually an ξ = const grid line which, because of grid warping in this region, is not aligned with the actual trailing edge. Figure 9 shows the streamwise velocity field using shaded contours and the in-plane velocity field using vectors at station 30. For clarity, only the velocity vectors at every other point are plotted. Examination of the velocity vectors reveals the counterclockwise primary vortex above the wing and a clockwise secondary vortex. In addition, the dark shaded area at approximately 75% span indicates the region of streamwise flow reversal mentioned earlier. Entrainment from the primary and secondary vortices produces a region of low pressure responsible for the reversed flow.

Shown in Fig. 10 is the complex eigenvalue field for the delta wing at station 30. In this figure, as well as those that follow, several regions of the flowfield have been denoted alphabetically to aid the discussion of the results. The complex eigenvalue field indicates the existence of the primary vortex (region A) as well as the secondary vortex (region B). Also indicated are the shear layer emanating from the leading edge (C and E) and the region of chordwise flow reversal (D). A small, unlabeled region of complex eigenvalues is also visible on the lower surface of the wing.

Figure 11 shows the intrinsic swirl parameter field computed using a convection velocity based on the normalized vorticity vector [see Eq. (27)]. Figure 12 shows the intrinsic swirl parameter field computed using a convection velocity based on the normalized real eigenvector [see Eq. (27)]. Figure 13 shows the intrinsic swirl parameter field computed using a convection velocity based on the normalized complex left eigenvectors [see Eq. (28)]. Figures 11–13 show a great deal of similarity as far as locating the most active swirling structures although the shading scales used in the three figures are

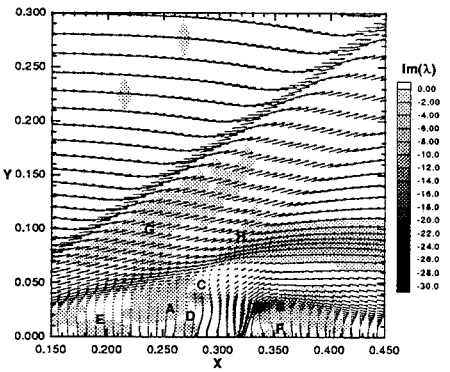

Fig. 6 Sonic jet in supersonic crossflow—velocity vectors and regions of complex eigenvalues.

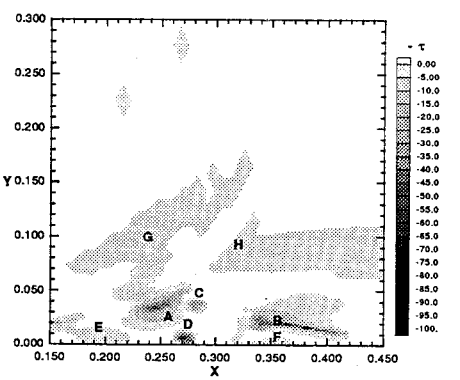

Fig. 7 Sonic jet in supersonic crossflow—intrinsic swirl parameter.

slightly different. All three show the location of the secondary vortex (B) as well as the "nearly recirculating" region in the shear layer (C). The major difference occurs in the core of the primary vortex (A) where Fig. 11 shows a distinct, two-lobed structure and Fig. 12 shows a double-lobed core. A secondary peak in the intrinsic swirl parameter also occurs in Fig. 13, although to a much smaller extent. It should be noted that the core region of the secondary vortex (B) as determined by the swirl parameter is located above the region suggested by the in-plane velocity vectors. Further examination shows that in the region indicated as being a core region by the intrinsic swirl parameter, the pressure and velocity magnitude both assume relative minima suggesting the presence of a vortex core.[18]

The region labeled D in Figs. 11-13 is located in the region of chordwise flow reversal (see Fig. 8) just ahead of one of the vortical structures on the upper surface of the wing. More significantly, this is the region between the two separation lines shown in Fig. 8. Examination of other streamwise stations ahead of station 30 verifies that, in fact, the intrinsic swirl parameter locates this region even when there is no chordwise flow reversal.

A final point to make about this sequence of figures concerns the region in the shear layer labeled E. The granularity of all of the plots in this region can most probably be attributed to a grid resolution problem. Although not shown here, the discrete mesh used for the calculation had cells of rather large aspect ratio and was quite crude in the general region of the shear layer. In addition to introducing inaccuracies in the original calculation, the grid may also introduce error in the derivative calculations used to evaluate the velocity gradient tensor. It should be stressed that in the figures shown here no smoothing of the data was performed.

We would like to conclude the discussion of the delta wing results with Fig. 14, which shows a plot of the intrinsic swirl parameter in the plane of the first grid point above the wing surface and in the perpendicular planes located at stations 20 and 30. Here, the convective velocity is defined using the left eigenvector as suggested by Eq. (28). There is a region of large magnitude intrinsic swirl parameter at the nose of the delta wing. The evolution of the primary and secondary vortices is evident from examination of the two perpendicular planes. As discussed in the preceding paragraph, the approach proposed

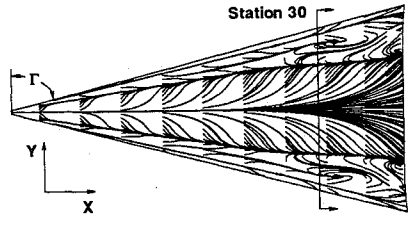

Fig. 8 Simulated surface oil flow for delta wing.

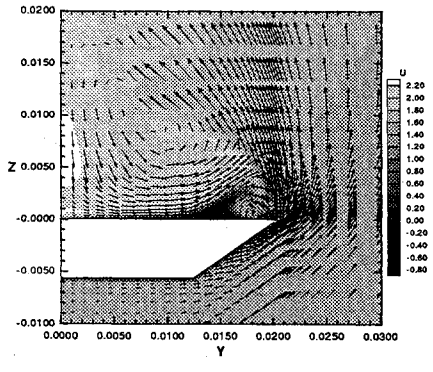

Fig. 9 Velocity field for delta wing station 30—shaded contours (streamwise component) and vectors (in-plane velocities).

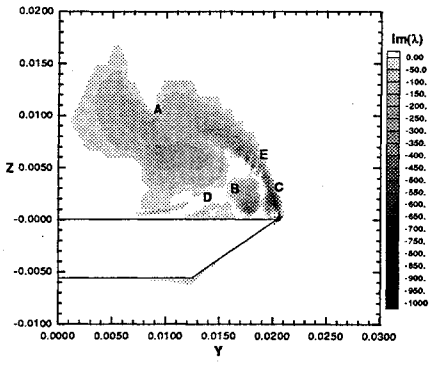

Fig. 10 Complex eigenvalue field—delta wing station 30.

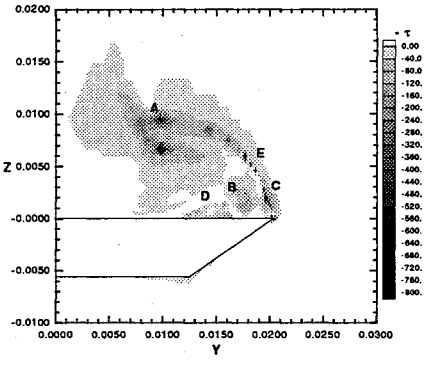

Fig. 11 Intrinsic swirl parameter with convection velocity based on vorticity vector—delta wing station 30.

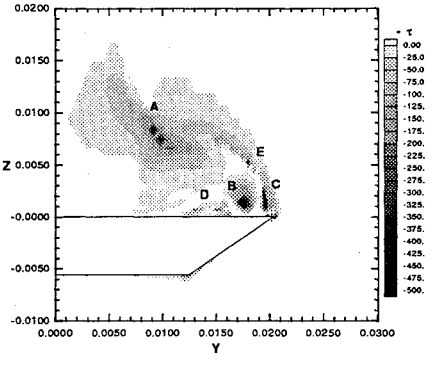

Fig. 12 Intrinsic swirl parameter with convection velocity based on right eigenvector—delta wing station 30.

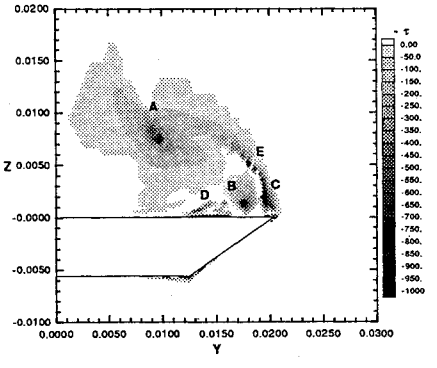

Fig. 13 Intrinsic swirl parameter with convection velocity based on left eigenvector—delta wing station 30.

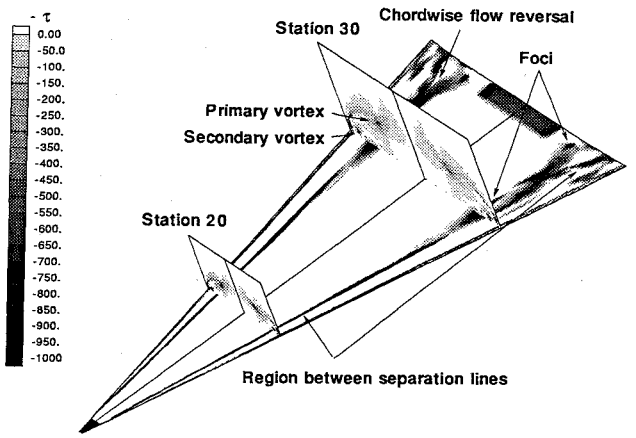

Fig. 14 Intrinsic swirl parameter for delta wing.

here does locate the region between the separation lines on the upper surface of the wing. Also prominent in the plane above the wing are the regions of chordwise flow reversal and the foci of the vortical flow regions. The dark region passing through the symmetry plane appears to be the result of the flow deflecting upward just ahead of the region and deflecting downward near the trailing edge as if to initiate swirling motion.

Additional Applications

In addition to applications in flowfield visualization, these eduction results and the swirl properties surfacing in the complex eigenvalue condition indicate that there may be significant potential for flowfield control using these ideas. Equation (12) indicates what velocity gradients must simultaneously exist for a two-dimensional flow to swirl. Proper manipulation of the normal strain rates appearing in Eq. (12) may inhibit or induce, as desired, the occurrence of complex eigenvalues and, therefore, swirling-type motion. This would seem to have application in mixing problems where the swirling motion is desirable. In addition, it would appear that this behavior could be exploited to suppress transition to turbulent flow since a possible definition of turbulence is an unsteady flow of convecting eddies. In our interpretation, an eddy would be defined as a contiguous region of fluid throughout which two of the eigenvalues of the velocity gradient tensor are complex.

Summary

The complex eigenvalues are useful as an eduction technique for identifying swirling structures in real flowfields. In particular, the intrinsic swirl parameter appears to be a very powerful tool for locating the core regions of vortices. The technique is well understood for two-dimensional applications. For three-dimensional applications, there is a question of uniqueness involving the selection of the convection velocity that is unresolved at this time. However, the utility of the method is apparent from the results shown here. More generally, the basic ideas contained here suggest the existence of a fluid property that we have termed intrinsic swirl. This new property may be useful for control of fluid motion in many practical problems.

Acknowledgments

The partial support of the Texas Higher Education Coordinating Board's Advanced Research Program, Grant 003656-058, is gratefully acknowledged. We would also like to thank Phillip Webster at the Air Force Flight Dynamics Laboratory for providing the delta wing solution.

References

[1]Belie, R. G., "Some Advances in Digital Flow Visualization," AIAA Paper 87-1179, June 1987.

[2]Lasinski, T., Buning, P., Choi, D., Rogers, S., Bancroft, G., and Merritt, F., "Flow Visualization of CFD Using Graphics Workstations," AIAA Paper 87-1180, June 1987.

[3]Hesselink, L., and Helman, J., "Evaluation of Flow Topology from Numerical Data," AIAA Paper 87-1181, June 1987.

[4]Weston, R. P., "Color Graphics Techniques for Shaded Surface Displays of Aerodynamics Flow Field Parameters," AIAA Paper 87-1182, June 1987.

[5]Lugt, H. J., *Vortex Flow in Nature and Technology,* Wiley, New York, 1972.

[6]Truesdell, C., *The Kinematics of Vorticity,* Indiana Univ. Press, Bloomington, IN, 1954.

[7]Berdahl, C. H., and Strang, W. Z., "Behavior of a Vorticity-Influenced Asymmetric Stress Tensor in Fluid Flow," Air Force Wright Aeronautical Lab., AFWAL-TR-87-3929, Wright-Patterson AFB, OH, Oct. 1987.

[8]Perry, A. E., and Chong, M. S., "A Description of Eddying Motions and Flow Patterns Using Critical-Point Concepts," *Annual Review of Fluid Mechanics,* Vol. 19, 1987, pp. 125-155.

[9]Thompson, P. A., *Compressible Fluid Dynamics,* McGraw-Hill, New York, 1972.

[10]Strang, G., *Linear Algebra and Its Applications,* 2nd ed., Academic, New York, 1980.

[11]Aris, R., *Vectors, Tensors, and the Basic Equations of Fluid Mechanics,* Dover, New York, 1989.

[12]Smith, B. T., Boyle, J. M., Dongarra, J. J., Garbow, B. S., Ikebe, Y., Klema, V. C., and Moler, C. B., "Matrix Eigensystem Routine—EISPACK Guide," *Lecture Notes in Computer Science,* edited by G. Goos and J. Hartmanis, Vol. 6, Springer-Verlag, New York, 1986.

[13]Dongarra, J. J., Moler, C. B., Bunch, J. R., and Stewart, G. W., *LINPACK Users' Guide,* Society for Industrial and Applied Mathematics, Philadelphia, 1986.

[14]Roache, P. J., *Computational Fluid Dynamics,* Hermosa, Albuquerque, NM, 1982.

[15]Thompson, D. S., "Numerical Solution of a Two-Dimensional Jet in a Supersonic Crossflow Using an Upwind-Relaxation Scheme," AIAA Paper 89-1869, June 1989.

[16]Webster, W. P., and Shang, J. S., "Numerical Simulation of Reversed Flow over a Supersonic Delta Wing at High Angle of Attack," AIAA Paper 89-1802, June 1989.

[17]Pulliam, T. H., and Steger, J. L., "Implicit Finite-Difference Simulations of Three-Dimensional Compressible Flows," *AIAA Journal,* Vol. 18, No. 2, 1980, pp. 159-167.

[18]Yates, L. A., and Chapman, E. T., "Streamlines, Vorticity Lines, and Vortices," AIAA Paper 91-0731, Jan. 1991.